Biomechanical Rigidity and Quantitative Proteomics Analysis of Segmental Regions of the Trabecular Meshwork at Physiologic and Elevated Pressures

Janice A. Vranka,[1] Julia A. Staverosky,[1] Ashok P. Reddy,[2] Phillip A. Wilmarth,[2,3] Larry L. David,[2,3] Ted S. Acott,[1,3] Paul Russell,[4] and Vijay Krishna Raghunathan[5,6]

[1]Department of Ophthalmology, Casey Eye Institute, Oregon Health & Science University, Portland, Oregon, United States
[2]Proteomics Shared Resources, Oregon Health & Science University, Portland, Oregon, United States
[3]Department of Biochemistry and Molecular Biology, Oregon Health & Science University, Portland, Oregon, United States
[4]Department of Surgical and Radiological Sciences, School of Veterinary Medicine, University of California-Davis, Davis, California, United States
[5]Department of Basic Sciences, The Ocular Surface Institute, College of Optometry, University of Houston, Houston, Texas, United States
[6]Department of Biomedical Engineering, Cullen College of Engineering, University of Houston, Houston, Texas, United States

Correspondence: Janice Vranka, Casey Eye Institute, Oregon Health & Science University, 3181 SW Sam Jackson Park Road, Portland, OR 97239, USA; vranka@ohsu.edu.

Submitted: August 4, 2017
Accepted: December 5, 2017

Citation: Vranka JA, Staverosky JA, Reddy AP, et al. Biomechanical rigidity and quantitative proteomics analysis of segmental regions of the trabecular meshwork at physiologic and elevated pressures. *Invest Ophthalmol Vis Sci.* 2018;59:246–259. https://doi.org/10.1167/iovs.17-22759

Purpose. The extracellular matrix (ECM) of the trabecular meshwork (TM) modulates resistance to aqueous humor outflow, thereby regulating IOP. Glaucoma, a leading cause of irreversible blindness worldwide, is associated with changes in the ECM of the TM. The elastic modulus of glaucomatous TM is larger than age-matched normal TM; however, the biomechanical properties of segmental low (LF) and high flow (HF) TM regions and their response to elevated pressure, are unknown.

Methods. We perfused human anterior segments at two pressures using an ex vivo organ culture system. After extraction, we measured the elastic modulus of HF and LF TM regions by atomic force microscopy and quantitated protein differences by proteomics analyses.

Results. The elastic modulus of LF regions was 2.3-fold larger than HF regions at physiological (1×) pressure, and 7.4-fold or 3.5-fold larger than HF regions at elevated (2×) pressure after 24 or 72 hours, respectively. Using quantitative proteomics, comparisons were made between HF and LF regions at 1× or 2× pressure. Significant ECM protein differences were observed between LF and HF regions perfused at 2×, and between HF regions at 1× compared to 2× pressures. Decorin, TGF-β–induced protein, keratocan, lumican, dermatopontin, and thrombospondin 4 were common differential candidates in both comparisons.

Conclusions. These data show changes in biomechanical properties of segmental regions within the TM in response to elevated pressure, and levels of specific ECM proteins. Further studies are needed to determine whether these ECM proteins are specifically involved in outflow resistance and IOP homeostasis.

Keywords: biomechanics, trabecular meshwork, atomic forcy microscopy, proteomics, anterior segment

Glaucoma is a leading cause of blindness and affects over 67 million people worldwide.[1,2] Elevated IOP is the primary risk factor leading to glaucoma. Changes in the extracellular matrix (ECM) of the trabecular meshwork (TM) have been shown to be associated with glaucoma.[3,4] The TM is a filter-like tissue in the anterior segment of the eye and can be divided into separate regions based on location and function: the uveal and corneoscleral meshworks, and the juxtacanalicular region (JCT) which is directly adjacent to the inner wall endothelium of Schlemm's canal (SCE).[5] Due to a reliable homeostatic mechanism that keeps IOP within relatively narrow, acceptable limits throughout life, most individuals never suffer glaucoma.[6] These normal, corrective adjustments of the aqueous humor outflow resistance, which occur in direct response to sustained pressure changes, are defined as IOP homeostasis.[6] The ECM of the TM is involved in regulation of outflow resistance and, thus, IOP homeostasis.[7–13]

Cells in a tissue can sense and respond to the stiffness of their substratum, altering many cellular behaviors, such as proliferation, differentiation, apoptosis, organization, and migration.[14] Recent research has documented the connection between changes in the biomechanical properties of tissues with various end-stages of disease, such as fibrotic diseases and cancer.[15–17] The biomechanical properties and composition of the ECM affect cell behavior in profound ways, as has been shown in a wide range of tissue defects, as well as in animal models, where mutations in genes that encode integral components of the ECM result in embryonic lethality.[18,19] The mechanical cues of ECM stiffness sensed by the cell lead to signaling cascades that are linked to appropriate cellular responses.

It was shown previously by atomic force microscopy (AFM) that the apparent elastic modulus of glaucomatous TM is 20-fold greater than that of age-matched normal TM, suggesting an important link between tissue compliance and the disease.[20] In apparent contrast, using uniaxial tensile testing methods, circumferential elastic modulus was measured in human TM tissues at multiple pressures. A positive correlation was shown, whereby a greater uniaxial tensile modulus of the TM correlated with higher total outflow facility.[21] Another study by the same group showed that the circumferential uniaxial tensile elastic modulus of glaucomatous TM was less than that of normal TM and had no correlation with outflow facility.[22] These studies suggest a complex relationship between TM biomechanics and outflow facility. They also did not address outflow segmentation patterns, which will affect their assessment dramatically, and warrant a closer investigation, which is one of the aims of our study. We and others have demonstrated previously that outflow is segmental around the circumference of the eye (Vranka J, et al. *IOVS* 2013;54:ARVO E-Abstract 3566).[23–28] This segmental outflow, with regions of relatively lower and higher flow, complicates the understanding of molecular mechanisms regulating outflow facility. Biomechanical properties of the segmental regions of the TM and the effects of elevated pressure are unknown. We hypothesized that biomechanical and protein level differences exist between low flow (LF) and high flow (HF) segmental regions of the TM. We investigated stiffness in segmental outflow areas of the TM from tissues perfused at physiologic (1×) and elevated (2×) pressures for 24 and 72 hours to trigger the homeostatic corrective response, since mRNA levels of key ECM genes in the TM have been shown previously to change in response to elevated pressure.[6,10,29] We used advanced quantitative proteomics to identify differential levels of proteins from segmental regions of human TM tissues perfused at physiologic and elevated pressures for 72 hours.

Methods

Anterior Segment Perfusion Culture

Anterior segment perfusion culture is an established technique to study outflow facility ex vivo.[30] Use of human donor eye tissue was approved by the Oregon Health and Science University Institutional Review Board and experiments were conducted in accordance with the tenets of the Declaration of Helsinki for the use of human tissue. Human eye tissue was obtained postmortem from Lions VisionGift (Portland, OR, USA), and we obtained no information that could lead to identification of a tissue donor. Length of time from death to stationary culture was less than 48 hours and anterior segments initially were placed into serum-free stationary organ culture for 5 to 7 days to facilitate postmortem recovery.[31] The age range was 52 to 95 years and average age of the donors' eyes for all experiments in this study was 77.3 ± 8.7 years. Donor demographics are included in Supplementary Table S1. After stationary culture, human anterior segments were perfused with serum-free Dulbecco's modified Eagle's medium (DMEM; a 1:1 mixture of high and low glucose DMEM) containing 1% penicillin/streptomycin/Fungizone, at constant pressure (8.8 mm Hg) with an average flow rate of 1 to 9 μL/min, which is similar to normal physiologic rate and pressures (minus episcleral venous pressure) in vivo. Anterior segments were perfused continuously at 8.8 mm Hg pressure (or "1×"). In some cases anterior segments were elevated to 17.6 mm Hg (or "2×") perfusion pressure to produce a pressure challenge to trigger intraocular homeostatic responses[6] as noted in the Figure legends. During the final stage of perfusion, fluorescently-labeled amine-modified 200 nm Fluospheres or Cell Mask Orange (Thermo Fisher Scientific, Waltham, MA, USA) were diluted 1:1000 into PBS, vortexed vigorously, and 200 μL of that mixture was injected as a bolus directly in-line into the anterior segment organ culture and perfused for 1 hour. This time was adjusted to accommodate different flow rates such that approximately equal volumes of the tracer were perfused. Perfusion was stopped and anterior segments were imaged en face using a Leica DM500 microscope (Leica Microsystems, Buffalo Grove, IL, USA) before cutting into radial wedges of HF or LF regions. HF and LF regions were separated routinely based on relative fluorescence of the TM on a per eye basis. A representative image is shown in our previous study indicating HF and LF regions.[25] In the same study, relative fluorescence intensity was mapped across flow regions of the TM and plotted versus distance using ImageJ software.[25] For all eyes in this study, we measured the circumference of the TM using a protractor overlay of the whole eye en face image. The same overlay application was used to determine the number of degrees of that circumference that were HF or LF with the remainder considered intermediate flow (IF). Most normal eyes have approximately a third HF, a third LF, and a third IF regions, or rather, the intensity of HF regions represents the upper 30th percentile, the intensity of LF regions represents the lower 30th percentile, and the IF regions were everything in between. IF regions were not included. TM tissues then were dissected and used for subsequent analysis by AFM or quantitative proteomics. Data from individual eyes were combined where possible and representative images were used. The number of eyes used for each treatment is noted in the Figure legend and is included in Supplementary Table S1.

Atomic Force Microscopy and Determination of Elastic Modulus

After perfusion, labeling, and cutting of the anterior segments into wedges of HF or LF regions, tissues were placed in PBS and shipped overnight on ice to the AFM lab. Within less than 24 hours of perfusion, the TMs were dissected from the tissue wedges and mounted with the JCT/SCE inner wall facing up and the outer TM beams facing down. In brief, from wedges of anterior segments or corneoscleral rims, we remove any iridal remnants with a 22.5° stab blade coming in horizontally. Then, using a jeweler's forceps, we gently lifted the TM out, maintaining careful attention to orientation. This method was reported in detail by Tamm et al.[32] and described initially by our group,[20] in which the TM tissue dissection method was described in careful detail. More specifically, the dissected TM was maintained carefully so that the SC inner wall side was facing up to the AFM cantilever with the outer beam portion facing down. In numerous parallel TM samples, we used histologic staining of the tissues before and after the isolation process (see Fig. 1 of Last et al.[20]) to verify the sample orientation. This method also has been modified from the original sample mounting method[20] and includes a soft-clamping immobilizing retainer of tissue (SCIRT) retainer system.[33] Briefly, the sample was placed on a thin coating of Sylgard 527 (a dielectric silicone polymer), upon which a SCIRT is placed. The TM is accessible through a window within the SCIRT with the JCT/SCE side of the mounted TM tissue on top for the AFM measurements. As a result, the sample does not come in contact with any glue material, but is adhered firmly to the silicone polymer. Elastic moduli of the JCT/SCE face of the TM tissues were determined by AFM as described previously.[20,33,34] Elastic moduli measurements of TM tissues in this study generally were stiffer than those previously measured on cultured SC cells.[35] However, the cantilever tip shape, as well as the location along the cell

Investigative Ophthalmology & Visual Science

where the measurement is made (nucleus versus cytoplasm) have been shown to affect AFM measurements.[36] In addition, recent studies of SCE biomechanics by AFM in situ showed that the SCE cells themselves are very soft (0.34–0.36 kPa) compared to those grown on glass, although they did not know whether they were measuring HF or LF regions; thus, the SCE cells would have minimal impact on our measurements.[36,37] Briefly, force versus indentation curves were obtained using the MFP-3D Bio AFM (Asylum Research, Santa Barbara, CA, USA) coupled with a Zeiss Axio Observer inverted microscope (Carl Zeiss Meditec, Thornwood, NY, USA). Silicon nitride cantilevers (PNP-TR-50, nominal spring constant [κ] of 0.32 N/m and half angle opening of 35°; NanoAndMore, Lady's Island, SC) were modified by incorporation of a borosilicate bead (nominal radius, $R = 5$ μm; Thermo Fisher Scientific) at the free end of the cantilever; These colloidal probes were calibrated for deflection inverse optical lever sensitivity (Defl InvOLS) by indentation in HBSS on glass and then the actual spring constant of the cantilever was determined by the thermal method using the Asylum Research software. All samples were equilibrated in Hank's balanced salt solution (HBSS) for 30 minutes before obtaining measurements. For all samples, five force curves were obtained from at least seven different positions. Elastic modulus of each sample was obtained by fitting indentation force versus indentation depth of the sample with an overlay of the theoretical force based on the geometry-appropriate Hertz model for spherical tip as described previously.[38] All biologic samples were assumed as incompressible materials because of their high water content and, therefore, the Poisson's ratio was assumed to be 0.5.[39–43] Determining the accurate indentation depth across which the biologic sample behaves as a linear-elastic material is difficult from the F versus δ curves. Thus, the elastic regime of a viscoelastic tissue, where E is constant over a restricted indentation depth, was determined from a plot of E versus δ values.[44] Six biologic replicates from six different eyes were used for each region and condition. Elastic moduli were averaged for each condition and region. Since not all eyes were paired, they were treated as individual replicates and not considered as paired in the statistical analysis. The statistical test for stiffness differences was 1-way ANOVA with Sidak's multiple comparison correction computed using GraphPad Prism software (La Jolla, CA, USA). *P* values are indicated in the Figure legend for each comparison.

Tissue Lysis

TM tissues (four sets of 4 samples: 1× LF, 1× HF, 2× LF, 2× HF) were transferred individually to a tared 2 mL tube with 2.4 mm stainless steel beads and weighed. Samples were lysed by bead beating in 150 μL of 167 mM Triethyl ammonium bicarbonate (TEAB) using an Omni Bead Ruptor 24 Homogenizer (speed = 6, cycles = 3, cycle time = 1.0 min, dwell/pause = 1.0 min) followed by addition of 100 μL of 10% SDS, 0.5% deoxycholic acid (DCA) to the lysate and bead beating repeated as shown above. Lysed samples were centrifuged for 20 minutes at 16,000*g* at 4°C and supernatant transferred to a 1.5 mL lowbind Eppendorf tube. BCA assay (Thermo Fisher Scientific) was performed to determine protein concentration. Protein recovery ranged from 0.4% to 2.3% of wet weight of tissue.

Digestion

A total of 14 μg protein from eight samples and two pooled samples (1.75 μg × 8 samples) per TMT experiment (10 samples each) were e-FASP digested.[45] Briefly, samples were reduced with 1 M tris(2-carboxyethyl)phosphine (TCEP) by heating at 90°C for 10 minutes, transferred to a 30 kDa Amicon filter (EMD Millipore, Billerica, MA, USA) followed by buffer exchange into 8 M urea, 0.2% DCA, 100 mM TEAB. Samples were alkylated with Iodoactetamide at 37°C for 1 hour, buffer exchanged into digestion buffer (0.2% DCA, 50 mM TEAB, pH 8) and digested with trypsin (1:35 enzyme:substrate) overnight. Samples were centrifuged, the filtrate containing the peptides were extracted with ethyl acetate to remove DCA, dried, and taken for tandem mass tag (TMT) labeling.

TMT Labeling

Digested and dried samples (14 μg each) were dissolved in 25 μL 100 mM triethylammonium bicarbonate and labeled using TMT-10-plex reagents (Thermo Fisher Scientific). The manufacturer suggested protocol was used, except recommended amounts of each reagent were decreased by a factor of 4. Briefly, TMT labeling was done on 14 μg of peptides from each individual sample and the two pooled samples per TMT experiment. TMT 10-plex labeling reagents (0.8 mg) were each dissolved in 52 μL anhydrous acetonitrile (ACN). Each sample containing 14 μg of peptide in a 25 μL volume of TEAB buffer was combined with 12 μL of its respective 10-plex TMT reagent and incubated for 1 hour at room temperature. A pooled sample for normalization was prepared by combining 2 μL of each labeled sample, 2 μL of 5% hydroxylamine added, and the combined sample incubated for a further 15 minutes. The mixture then was dried down, dissolved in 5% formic acid, and 2 μg peptide analyzed by a single 2-hour liquid chromatography-tandem mass spectrometry (LC-MS/MS) method using an Orbitrap Fusion as described below. This run was performed to normalize the total reporter ion intensity of each multiplexed sample and to check labeling efficiency. The remaining samples were quenched by addition of 2 μL 5% hydroxylamine as above, then combined in a 1:1:1:1:1:1:1:1:1:1 mixture for each of two TMT experiments based on total reporter ion intensities determined during the normalization run, and dried down for 2-dimensional (2D)-LC-MS/MS analysis.

LC-MS/MS Analysis

TMT-labeled samples (46.3 μg per experiment) were reconstituted in 20 μL of HPLC water and separated by two-dimensional reverse-phase liquid chromatography (2D-LC) using a Dionex NCS-3500RS UltiMate RSLCnano UPLC system (Thermo Fisher Scientific). Each 20 μL biologic sample (46.3 μg) was injected onto a NanoEase 5 μm XBridge BEH130 C18 300 μm × 50 mm column (Waters Corporation, Milford, MA, USA) at 3 μL/min in a mobile phase containing 10 mM ammonium formate (pH 9). Peptides were eluted by sequential injection of 20 μL volumes of 14%, 17%, 20%, 21%, 22%, 23%, 24%, 25%, 26%, 27%, 28%, 29%, 30%, 35%, 40%, 50%, and 90% ACN in 10 mM ammonium formate (pH 9) at 3 μL/min flow rate. Bound peptides (Acclaim PepMap 100 μm × 2 cm NanoViper C18, 5 μm trap; Thermo Fisher Scientific) were diluted with mobile phase containing 0.1% formic acid at 24 μL/min flow. After 10 minutes of loading, the trap column was switched in-line to a PepMap RSLC C18, 2 μm, 75 μm × 25 cm EasySpray column (Thermo Fisher Scientific). Peptides then were separated at low pH using a 7.5%–30% ACN gradient over 90 minutes in mobile phase containing 0.1% formic acid at 300 nL/min flow rate. Each second dimension LC run required 2 hours for separation and re-equilibration, so each 2D LC-MS/MS method required 36 hours for completion. Tandem mass spectrometry data were collected using an Orbitrap Fusion Tribrid instrument configured with an EasySpray NanoSource (Thermo Fisher Scientific). Survey scans were performed in the Orbitrap mass analyzer (resolution = 120,000), and data-dependent MS2 scans performed in the linear ion trap using

Investigative Ophthalmology & Visual Science

collision-induced dissociation (normalized collision energy = 35) following isolation with the instrument's quadrupole. Reporter ion detection was performed in the Orbitrap mass analyzer (resolution = 60,000) using MS3 scans following synchronous precursor isolation (SPS) of the top 10 ions in the linear ion trap, and higher-energy collisional dissociation in the ion-routing multipole (normalized collision energy = 65). The MSn scans used default automatic gain control ion targets provided in the TMT SPS template and variable numbers of MS2 scans between survey scans to automatically optimize data collection. Singly charged precursor ions were excluded and dynamic exclusion settings were 10 PPM m/z tolerances for 30-second durations.

TMT Data Analysis

Raw instrument files were processed using Proteome Discoverer version 1.4.1.14 (Thermo Fisher Scientific). For each of the TMT experiments, raw files from the 18 fractions were merged and searched with the SEQUEST HT search engine with a human Swiss-Prot protein database (canonical sequences) downloaded from www.uniprot.org (in the public domain) in July 2015 (20,193 entries). Searches were configured with static modifications for the TMT reagents (+229.163 Da) on lysines and N-termini, carbamidomethyl (+57.021 Da) on cysteines, dynamic modifications for oxidation of methionine residues (+15.9949 Da), parent ion tolerance of 1.25 Da, fragment mass tolerance of 1.0005 Da, monoisotopic masses, and trypsin cleavage (maximum two missed cleavages). Searches used a reversed sequence decoy strategy to control peptide false discovery and identifications were validated by Percolator software.[46]

Search results and TMT reporter ion intensities were exported from Proteome Discoverer as text files and processed with in-house Python scripts. Only peptide spectrum matches (PSMs) uniquely matching a single protein entry with q scores < 0.05, accurate masses within 10 PPM, and trimmed average reporter ion peak height greater than 500 were used for quantification. The individual reporter ion intensities from all unique PSMs were summed to create total protein intensities. We used an experimental design and normalization procedure called internal reference scaling (IRS) to handle the two 10-plex TMT experiments. This method is described byPlubell et al. in detail.[47]

Differential protein abundances between groups were determined by comparing the IRS-normalized total reporter ion intensities using the Bioconductor package edgeR.[48] EdgeR was developed for serial analysis of gene expression data but its modeling is flexible enough to handle a variety of other data types, such as TMT reporter ions. EdgeR has self-contained multiple testing corrections and false discovery rate evaluation, as are used commonly in large sample comparisons. Additional data normalizations,[49] and Benjamini-Hochberg multiple testing corrections were performed within edgeR. Percolator validation step uses a reversed sequence decoy strategy to control for peptide false discovery. Protein annotations from UniProt Swiss-Prot database records for the quantified proteins were added using in-house scripts. The sample size for the proteomics experiments was $n = 4$ biologic replicates, where the values from the same treatment and region were averaged across the replicates to determine the fold change values. Proteomics results for all differential level candidates are listed in Supplementary Table S2. The mass spectrometry proteomics data have been deposited to the ProteomeXchange Consortium (http://proteomecentral.proteomexchange.org, in the public domain) via the PRIDE partner repository[50] with the dataset identifier PXD006424. The ProteomeXchange submission contains complete proteomics identification and quantification results.

Gene Ontology using the Panther Classification System

Proteins identified from proteomics analyses were classified by the Gene Ontology PANTHER classification system.[51–56] Gene Ontology is defined as the framework for the model of biology and classifies functions along three aspects: molecular function (molecular activities of gene products), cellular component (where gene products are active), and biologic process (pathways and larger processes made up of the activities of multiple gene products (details can be found at: http://geneontology.org/ and http://www.pantherdb.org/, in the public domain).

Western Blotting

TM tissues from four or five donor eyes were extracted from HF and LF regions from perfused anterior segments and placed into a chaotropic buffer (2% SDS, 2 M urea, 14% sucrose, 1mM NaF) with a complete protease inhibitor cocktail tablet (Roche, Indianapolis, IN, USA). Tissues were homogenized using a mini-dounce apparatus (Squisher, Zymo Research, Irvine, CA, USA) and then centrifuged at 15,000*g* for 15 minutes to pellet residual debris. Supernatants were removed to a fresh tube and total protein was quantified by the bicinchoninic acid (BCA) protein assay kit (Thermo Fisher Scientific). Equal amounts of total protein (15 μg per lane) were combined in a 4× SDS-PAGE sample buffer and loaded on 4% to 20% gradient SDS-PAGE gels under reducing conditions and transferred to polyvinylidene difluoride (PVDF) membranes. Immunoblots were probed with the following antibodies: anti-decorin (Developmental Studies Hybridoma Bank; University of Iowa, Iowa City, IA, USA), anti-thrombospondin-1 and -4, and anti-MMP3 (all from Antibody Verify, Las Vegas, NV, USA). Secondary antibodies were IRDye 700–conjugated anti-rabbit and IRDye 800-conjugated anti-mouse (Rockland Immunochemicals, Gilbertsville, PA, USA). Immunoblots were imaged using the Odyssey infrared imaging system (Licor Biosciences, Lincoln, NE, USA), which also generated a digital image of the membrane. Pixel density of the gel bands in each lane were quantitated using ImageJ software (https://imagej.nih.gov/ij/; provided in the public domain by National Institutes of Health [NIH], Bethesda, MD, USA) following background correction. ANOVA was used to determine significance, where $P < 0.05$ was considered significant. Images shown are representative of all biologic replicates ($n = 3$).

Immunohistochemistry and Confocal Microscopy

At the end of perfusion, whole anterior segments were imaged en face for fluorescent labeling using a Leica DM500 microscope (Leica Microsystems, Buffalo Grove, IL, USA) before cutting into radial wedges of HF or LF regions. TM tissue intended for immunohistochemistry and confocal imaging, was immersion-fixed in 4% paraformaldehyde/PBS for 1 hour at 25°C. Frontal sections then were cut with a single-edged razor blade perpendicular to the ocular surface, resulting in a section tangential to the corneoscleral limbus that bisects Schlemm's canal as described previously.[11,24,25,57,58] Tissues were incubated in CAS-Block, a universal blocking reagent to saturate the nonspecific binding sites (Invitrogen, Grand Island, NY, USA), for 1 hour at room temperature, and then incubated overnight at 4°C with one or more of the following antibodies (also listed in Supplementary Table S3): anti-decorin (Developmental Studies Hybridoma

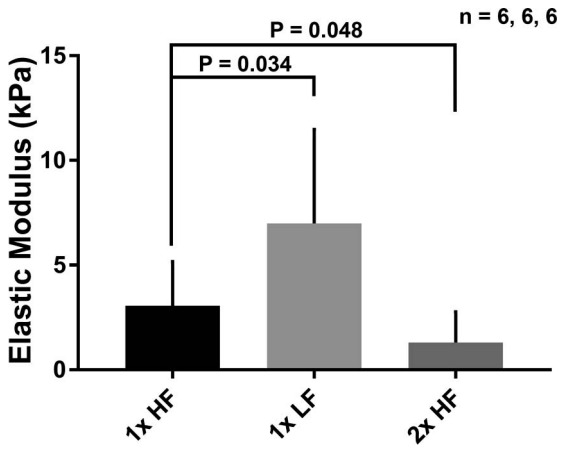

Figure 1. Elastic modulus by AFM of segmental flow regions of the TM. HF and LF regions of the TM perfused at physiologic (1×) or at elevated (2×) pressure for 24 hours; HF regions of the TM perfused at 1× were significantly softer than LF regions perfused at 1× ($P = 0.034$). HF regions perfused at 1× pressure were significantly stiffer than HF regions perfused at 2× pressure for 24 hours ($P = 0.048$); $n = 6$ biological replicates from six individual eyes for all conditions.

Bank; University of Iowa), anti-lumican, anti-dermatopontin, anti-TGFBI, and anti-thrombospondin 4 (all from Antibody Verify, Las Vegas, NV, USA). Primary antibodies were detected with either Alexa-Fluor 488- or 647-conjugated anti-mouse or anti-rabbit secondary antibodies (Thermo Fisher Scientific). Tissue wedges were placed on 0.17 mm Delta T cover glass bottom culture dishes from Bioptechs, Inc. (Butler, PA, USA) in Slowfade Gold antifade reagent with 4′,6-diamidino-2-phenylendole (DAPI; Invitrogen), and imaged by confocal microscopy using an Olympus FV1000 microscope. Optical sections were acquired using sequential scanning in separate laser channels. Image acquisition settings and number of optical sections in a stack were kept constant when comparing images. Images shown are representative of all biologic replicates ($n = 3$).

Results

Elastic Modulus of Segmental Flow Regions

Perfused anterior segment organ culture, an established technique used in the study of outflow facility ex vivo, was used.[30] Human donor eyes were perfused at either physiologic (1×) or at elevated (2×) pressure. TM tissues were dissected from perfused anterior segments and force displacement curves were obtained by atomic force microscopy to determine the elastic moduli of HF and LF regions of the deepest 1 to 2 μm of the JCT region of the TM. Results are shown in Figure 1, where the elastic modulus was shown to be significantly larger in the 1× LF regions compared to the 1× HF regions ($P = 0.0338$) and those of the 1× HF regions were significantly larger than in the HF regions perfused at 2× pressure for 24 hours ($P = 0.0480$). In terms of fold differences between segmental regions, when TM tissues were perfused at physiologic (1×) and elevated (2×) pressures, the mean elastic modulus of LF regions was 2.29- and 7.3-fold, respectively, larger than that of HF regions (6.99 vs. 3.05 kPa, respectively, and 9.67 vs. 1.31 kPa, respectively; Table 1). When TM tissues were perfused at elevated pressure for 72 hours, the mean elastic modulus of LF regions was 3.53-fold larger than that of HF regions (8.77 vs. 2.49 kPa, respectively; Table 1). Thus, HF regions were consistently more compliant than LF regions, especially when perfusion pressure was elevated for sufficient time to trigger IOP homoestatic adjustments.

Table 1. Elastic Modulus (kPa) of Segmental Regions of Human TM Tissue as Measured by Atomic Force Microscopy (AFM)

Perfusion Pressure	LF, kPa		HF, kPa		Fold Difference
	Mean*	SEM	Mean*	SEM	LF/HF
1×	6.99	1.83	3.05	0.86	2.3
2× (24 hr)	9.67	4.43	1.31	0.59	7.4
2× (72 hr)	8.77	1.98	2.49	0.56	3.5

* $n = 6$ biologic replicates. LF, segmental low; HF, high flow.

Elevated Pressure Induces Changes in the Elastic Modulus Within Each Flow Region

Smaller fold changes in elastic moduli were seen when comparing the same flow regions across different pressure conditions. For example, LF regions perfused at 2× pressure for 24 and 72 hours were stiffer than those perfused at 1× pressure (9.67 vs. 6.99 kPa, respectively [1.38-fold larger] and 8.77 vs. 6.99 kPa, respectively, [1.25-fold larger]; Table 1). Though these values were observed consistently across all samples tested, they were not statistically different. The elastic modulus of HF regions were 2.3- and 1.2-fold lower at 24 and 72 hours of 2× pressure, respectively, than those at 1× pressure (Table 1); the 24-hour 2× pressure was significantly different compared to the 1× pressure ($P = 0.048$). Table 1 shows that perfusion at elevated pressure induces opposite effects in HF and LF regions at 24 hours, where HF regions become more and LF regions less compliant.

Analysis of Differential Protein Levels Shows Cellular Components, Molecular Function, and Biologic Processes Associated With Segmental Outflow and Pressure-Induced Effects

TM tissues extracted from perfused anterior segments were mechanically disrupted and lysed before the subsequent steps of trypsin digestion, labeling, and analysis by mass spectrometry (as outlined in Fig. 2). Isobaric TMT labeling was used with high-resolution mass spectrometry to allow separate protein level measurements of 10 biologic samples per TMT experiment. LF and HF regions from physiologic pressure ($n = 4$) were compared to those from 72-hour high pressure perfusion ($n = 4$) for a total of 16 biologic samples. A study design using repeated measurements of standards created from pooling all biologic samples, after each had been labeled uniquely, allowed extended multiplexing from two TMT experiments to accommodate all samples. The first TMT experiment identified 3128 proteins (2 or more peptides per protein) and the second identified 3220 proteins. The union of identifications was 3730 total proteins, and the intersection of the identifications was 2628 proteins. The IRS method to combine data across multiple TMT experiments is restricted to the proteins observed in each TMT experiment, so 2628 proteins could be tested for differential levels.

Comparisons were made across different pressure conditions and flow regions to identify differential protein levels. Only two of the four possible comparisons reproducibly yielded a set of proteins whose differential levels were statistically significant with P value based false discovery rates (FDR) of less than 0.10. In the 2× LF versus 2× HF comparison, 11 proteins were present at significantly different levels, whereas in the 1× HF versus 2× HF comparison, 299 proteins

Investigative Ophthalmology & Visual Science

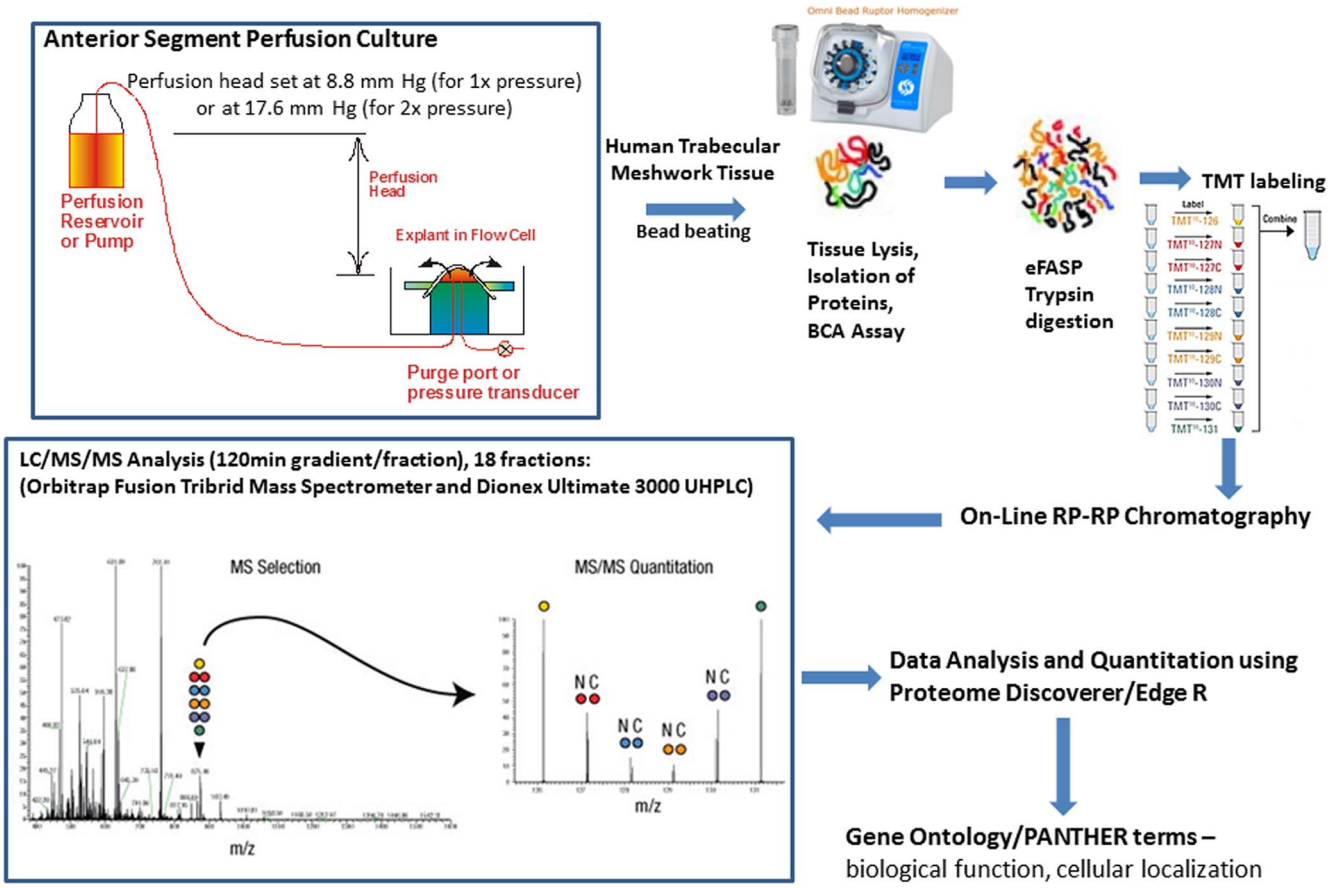

Figure 2. Experimental flow chart for identification of proteins in human TM. Human anterior segments were perfused in organ culture at 1× or 2× pressure (72-hour). After perfusion and labeling to identify flow regions, the TM tissue was extracted, homogenized and lysed before BCA quantitation and trypsin digestion. Equal amounts of total protein from each sample were labeled with individual TMTs (126-131, 10-plex) and then were combined for LC/MS/MS analysis. Reporter ions from the isobaric tags were used to quantitate relative peptide intensities, and peptides were identified from fragment ion sequencing. Differential protein levels were identified and proteins were classified based on their gene ontologies (UniprotKB database).

were at significantly different levels. In the other two comparisons, namely, 1× LF versus 1× HF and 1× LF versus 2× LF, we were not able to identify proteins that were at different levels between biologic replicates (statistically significant proteins identified by proteomics analysis are listed in Supplementary Table S2). Both sets of identified differential level protein candidates were classified using the Gene Ontology PANTHER classification system, which provides a framework of biologic systems based on three domains: molecular functions are the molecular activities of gene products, cellular components are where those gene products are active, and biologic process is the pathway or process that makes up the activities of multiple gene products. Cellular localization was determined for the two sets of protein candidates, the 2× LF versus 2× HF and 1× HF versus 2× HF comparisons, and a majority were either part of the cell (12.5% and 39.4%, respectively), ECM (37.5% and 4.1%, respectively), or residing in the extracellular region (50% and 6.2%, respectively; Fig. 3A). The molecular functions of the proteins from both candidate sets was determined to be predominantly that of binding activity (60% and 23.2%, respectively) and catalytic activity (40% and 54.2%, respectively; Fig. 3B).

Both sets of proteins found at differential levels shared multiple biologic processes, including biologic adhesion, cellular component organization, developmental process, immune process, metabolic process, multicellular organism, and response to stimulus (Fig. 4A). Protein candidates in both data sets were grouped into protein class according their gene ontologies (Fig. 4B). The predominant protein class of the 2× LF versus 2× HF comparison was ECM (33%), followed by receptor (33%), and signaling (16.7%), whereas for the 1× HF versus 2× HF comparison, the predominant protein class was oxidoreductase (25.2%), followed by transferase (14.3%), and hydrolase at 9.7% (Fig. 4B). Several cell-based proteins found at differential levels in the 1× HF versus 2× HF data set included key signaling proteins, growth factors, and cell adhesion molecules (see Supplementary Table S2 for full proteomics data sets). Panther analyses for the 2× LF versus 2× HF comparison may be less reliable due to the small number of differential level candidates.

Differential Levels of ECM Proteins are Found in Segmental Flow Regions and in Response to Elevated Pressure

ECM proteins of the TM are known to be involved critically in the aqueous outflow resistance and also were the predominant class of proteins identified to be at differential levels in the 2× LF versus 2× HF comparison (Table 2). Approximately 11% (33 of 299) of the proteins identified at differential levels in the 1× HF versus 2× HF comparison were ECM proteins (Table 3). The ECM proteins from both data sets were classified further based on the signaling pathways with which they were associated. The integrin signaling pathway was the dominant pathway for

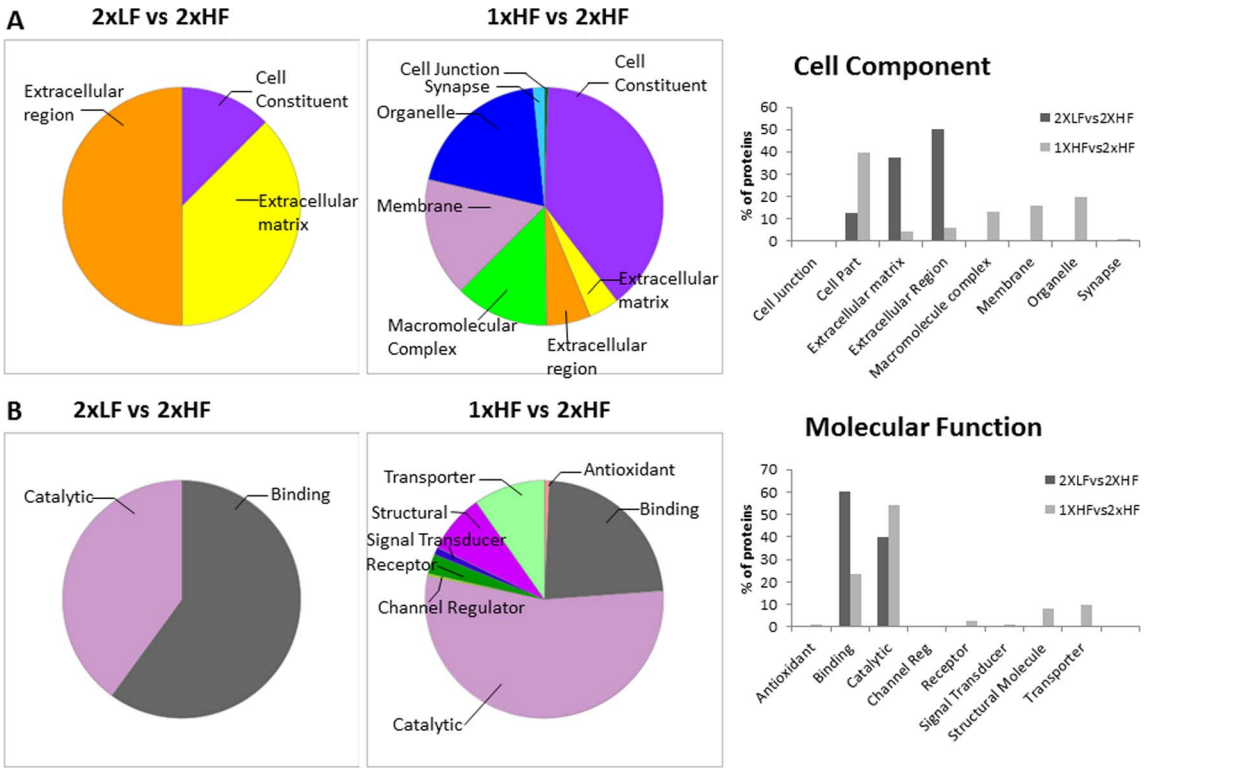

Figure 3. Gene ontology classification. (**A**) Cellular components. (**B**) Molecular function. Differential levels of proteins were identified by proteomics analysis and grouped into two comparisons: 2× LF versus 2× HF (11 candidate proteins) and 1× HF versus 2× HF (299 candidate proteins; See Supplementary Table S2 for the complete list of proteins). The resultant proteins were classified as either cellular component (**A**) or molecular function (**B**) and are represented in pie charts and bar graphs as a percentage of the total number of proteins identified.

the 1× HF versus 2× HF (37.5%) and 2× LF versus the 2× HF (50%; Fig. 4C) groups. Inflammation mediated by chemokine and cytokine signaling pathway was 50% for the 2× LF versus the 2× HF comparison, whereas the TGF-β (12.5%), p53 (12.5%), plasminogen activating (12.5%), CCKR (12.5%), and Alzheimer-presenilin (12.5%) pathways were associated with the remainder of the ECM proteins identified in the 1× HF versus 2× HF comparison. Interestingly, the two comparisons had in common a small group of seven ECM proteins, including decorin, keratocan, TGF-β-induced protein ig-h3, lumican, dermatopontin, thrombospondin 4, and MAM domain-containing protein 2. These seven proteins were further grouped based on their gene ontology terms into ECM (40%), receptor (30%), signaling (20%), and cell adhesion (10%) molecules (data not shown).

ECM Proteins Exhibit Differential Expression and Localization in Perfused TM Tissues

Western blots of TM tissues were performed to confirm select proteomics candidate proteins (Fig. 5). Stromelysin (MMP3) was found at slightly higher levels in the 1× HF regions compared to the 2× HF regions, as was shown in the proteomics data comparison. Likewise, decorin was found at higher levels in the 1× HF regions compared to the 2× HF regions, and at slightly higher levels in the 2× LF regions compared to the 2× HF regions, as was shown in the proteomics data comparisons (Fig. 5). Thrombospondin 1 and 4 also were detectable in all tissues. Densitometry was used to quantitate differences seen on the Western blots (Fig. 5). Immunohistochemistry was performed on perfused TM

Table 2. ECM Protein Candidates Identified at Differential Levels in 2× LF Versus 2× HF Regions, as Determined by Isobaric Tagging Quantitative Proteomics

Primary Protein Name	UniProt Link†	Identifier	FoldChange (2× LF/2× HF)	FDR*
Keratocan (KTN)	O60938	KERA_HUMAN	12.05	3.84E-08
Decorin	P07585	PGS2_HUMAN	7.40	2.75E-06
TGF-β–induced protein ig-h3 (Beta ig-h3)	Q15582	BGH3_HUMAN	7.10	6.09E-05
Lumican	P51884	LUM_HUMAN	6.05	8.55E-06
MAM domain-containing protein 2	Q7Z304	MAMC2_HUMAN	6.02	0.003565
Thrombospondin-4	P35443	TSP4_HUMAN	4.09	0.022446
Collagen α-3(VI) chain	P12111	CO6A3_HUMAN	3.54	0.025776
Collagen α-1(VI) chain	P12109	CO6A1_HUMAN	3.39	0.088031
Dermatopontin	Q07507	DERM_HUMAN	2.44	0.011499

* $n = 4$ biologic replicates; FDR < 0.10.
† www.uniprot.org/uniprot.

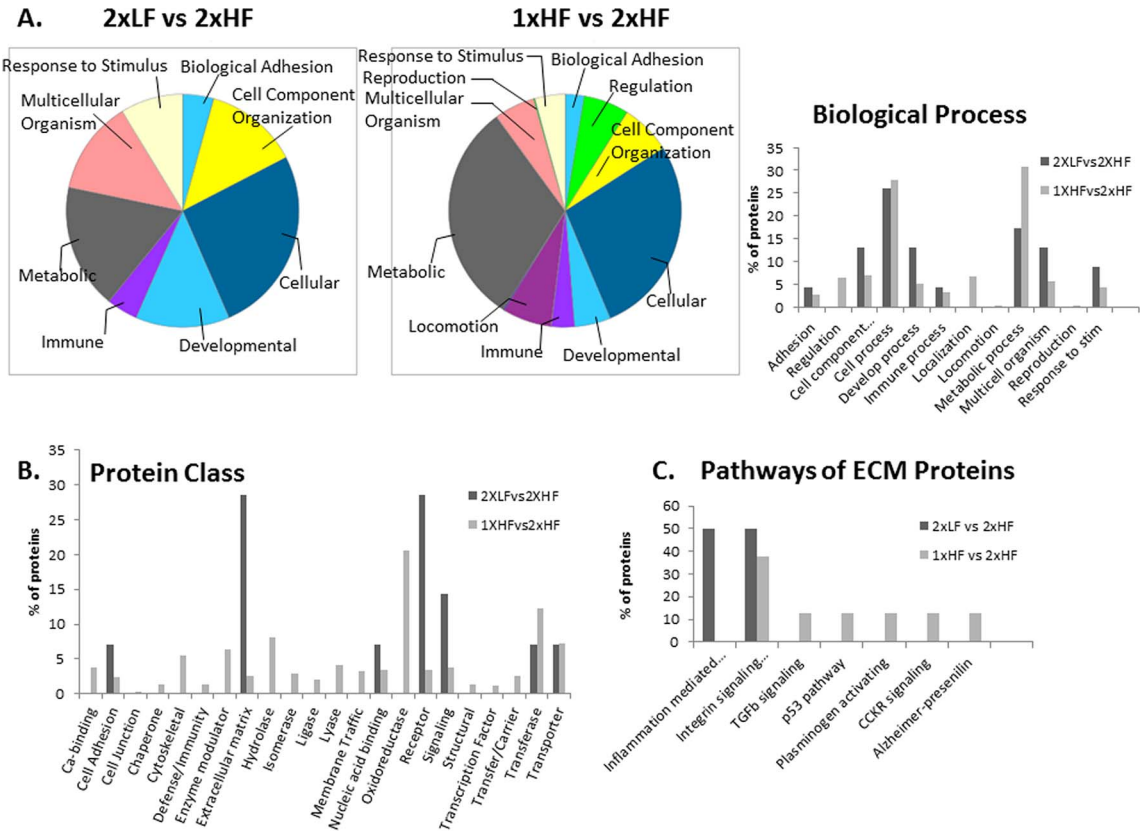

Figure 4. Gene ontology classification. (**A**) Biological Process. (**B**) Protein class. (**C**) Pathways of ECM proteins. Proteins identified by proteomics analysis were classified based on biological process (**A**) or by protein class (**B**) based on percentage of total number of proteins identified in each data set comparison (11 candidate proteins in the 2× LF versus 2× HF comparison, and 299 candidate proteins in the 1× HF versus 2× HF comparison.) The ECM proteins from each comparison were classified based on the pathways they are associated with (**C**). Only the integrin signaling pathway was shared between the two comparisons of ECM proteins.

tissues using antibodies to selected candidates from the proteomics data to show their localization (Fig. 6). These images show localization differences between proteins within regions of Schlemm's canal, juxtacanalicular TM tissue (JCT), and into the corneoscleral TM. Decorin localized primarily to the JCT and inner wall of Schlemm's canal and appeared to be directly under or adjacent to cells (Figs. 6A, 6B). Lumican was localized to the JCT region and along the inner wall of Schlemm's canal in a fibrillar staining pattern (Figs. 6C, 6D), whereas TGF-β–induced protein (TGFBI) localized around inner wall cells and along the trabecular beams (Figs. 6E, 6F). Dermatopontin also localized around or adjacent to cells in the JCT and corneoscleral TM regions (Figs. 6G, 6H), whereas thrombospondin 4 was somewhat punctate in appearance and more generally localized along the inner wall of Schlemm's canal and along the TM beams.

In summary, of all the ECM proteins identified by proteomics analyses, matricellular proteins and small leucine-rich proteoglycans (SLRPs) are disproportionately represented (overlapping area in Fig. 7). Relatively few structural ECM proteins were identified to be at differential levels—of these type VI collagen was identified to be at higher levels in 2× LF compared to 2× HF regions and type II collagen was at higher levels in the 1× HF compared to the 2× HF regions. Matrix metalloproteinases, matrix gla protein, and other ECM proteins were at differential levels in the 1× HF regions compared to 2× HF regions; however, the overlapping ECM proteins common to both data sets are predominantly SLRPs and matricellular proteins (Fig. 7).

Discussion

Biomechanical cues and cellular responses in the ECM are critical to maintain proper function of many tissues. The biomechanical properties of the TM are thought to contribute to the dynamic regulation of IOP, in response to local changes in pressure and, more generally, in aging and disease.[34,59–61] Changes due to aging have been observed in the ECM of the TM and include an increase in the thickness of the elastic fiber network, presumably affecting the biomechanical properties of the tissue.[4] These effects in the TM are even more extreme in the various forms of glaucoma, where additional ultrastructural effects are apparent.[3,4,20,60,62–64] ECM stiffness also is known to have a considerable role in regulating cell behavior in the TM.[29,34,59,65] In this study, we used AFM to determine the biomechanical properties of the segmental regions of the TM under physiologic and elevated pressure to mimic in vivo conditions of high IOP, which triggers changes in the outflow resistance to restore IOP to appropriate levels.[6] HF regions, considered to be areas of active filtration, were softer than LF regions and had smaller elastic moduli. When perfused at elevated pressure, the HF regions were softer than HF regions perfused at 1× pressure, and LF regions were stiffer than LF regions perfused at 1× pressure, as measured by AFM. The stiffness difference between the 1× LF and 1× HF regions was statistically significant, as was the difference between the 1× HF and 2× HF regions at 24 hours. These data suggest that tissue biomechanics and specific molecular components of the ECM within the human TM are associated with features of outflow, since LF regions are stiffer and have less active flow

Table 3. ECM Proteins Identified at Differential Levels in 1× HF versus 2× HF Regions, as Determined by Isobaric Tagging Quantitative Proteomics

Primary Protein Name	UniProt Link†	Identifier	FoldChange (1× HF/2× HF)	FDR*
Keratocan (KTN)	O60938	KERA_HUMAN	8.23	0.007052
Tenascin-N (TN-N)	Q9UQP3	TENN_HUMAN	4.32	0.096441
Lumican	P51884	LUM_HUMAN	4.26	0.013861
TGF-β–induced protein ig-h3 (β ig-h3)	Q15582	BGH3_HUMAN	4.24	0.060582
Decorin	P07585	PGS2_HUMAN	4.04	0.020587
MAM domain-containing protein 2	Q7Z304	MAMC2_HUMAN	3.86	0.039773
Stromelysin-1 (SL-1)	P08254	MMP3_HUMAN	3.11	0.008771
Spondin-1	Q9HCB6	SPON1_HUMAN	3.05	0.0385
Pleiotrophin (PTN)	P21246	PTN_HUMAN	2.96	0.001423
Matrix Gla protein (MGP)	P08493	MGP_HUMAN	2.86	0.05715
Thrombospondin-4	P35443	TSP4_HUMAN	2.78	0.062538
PEX	P08253	MMP2_HUMAN	2.58	0.026522
Chondrocalcin	P02458	CO2A1_HUMAN	2.55	0.009399
Thrombospondin-1	P07996	TSP1_HUMAN	2.43	0.005685
Extracellular superoxide dismutase [Cu-Zn] (EC-SOD)	P08294	SODE_HUMAN	2.32	0.0385
Dermatopontin	Q07507	DERM_HUMAN	2.26	0.036419
Pappalysin-1	Q13219	PAPP1_HUMAN	2.21	0.006052
Stromelysin-2 (SL-2)	P09238	MMP10_HUMAN	2.13	0.089442
Bone morphogenetic protein 5 (BMP-5)	P22003	BMP5_HUMAN	2.10	0.073513
Metalloproteinase inhibitor 1	P01033	TIMP1_HUMAN	2.00	0.028854
Latent-TGF-β–binding protein 2 (LTBP-2)	Q14767	LTBP2_HUMAN	1.81	0.029477
Cathepsin G (CG)	P08311	CATG_HUMAN	−1.75	0.073513
Tensin-1	Q9HBL0	TENS1_HUMAN	−1.79	0.063357
Nidogen-2 (NID-2)	Q14112	NID2_HUMAN	−1.80	0.097919
Beta-dystroglycan	Q14118	DAG1_HUMAN	−1.82	0.031572
Integrin-linked protein kinase	Q13418	ILK_HUMAN	−1.92	0.064457
Nidogen-1 (NID-1)	P14543	NID1_HUMAN	−2.02	0.035074
Integrin α-7 70 kDa form	Q13683	ITA7_HUMAN	−2.11	0.026389
Neural cell adhesion molecule L1 (N-CAM-L1; NCAM-L1)	P32004	L1CAM_HUMAN	−2.21	0.091098
Sarcospan	Q14714	SSPN_HUMAN	−2.39	0.073513
Cell surface glycoprotein MUC18	P43121	MUC18_HUMAN	−2.52	0.003195
Neural cell adhesion molecule 2 (N-CAM-2; NCAM-2)	O15394	NCAM2_HUMAN	−3.77	0.044638
Basal cell adhesion molecule	P50895	BCAM_HUMAN	−4.04	0.000164

* $n = 4$ biologic replicates; FDR < 0.10.
† www.uniprot.org/uniprot.

whereas HF regions are more compliant and have more active flow. Our elastic moduli results appear to be opposite to those reported by Camras et al.,[21] who showed that facility is higher in stiffer tissues.[21] The primary reason for this discrepancy is likely due to fundamental differences in the methods used to measure elastic moduli. Camras et al.[21] reported their values from uniaxial tensile testing, wherein the whole TM tissues were stretched in the circumferential direction. In contrast, we used AFM, where the tissue is indented only in the 1 to 2 μm of the inner wall side of the JCT and was indented perpendicular (i.e., radial), compared to the orientation of that study. Further, AFM provides information of local contributions to elastic modulus, such as micro HF or LF regions, while tensile measurements yield values for the entire piece of tissue, which will contain a heterogeneous mix of HF and LF regions. It is worthwhile to note that, under normal conditions, the TM is subjected to radial and circumferential stress and pressure stress from fluid continuously flowing across it. To our knowledge, quantification of radial stress on the TM in vivo or ex vivo has not been performed yet. McKee et al.[38] and Raghunathan et al.[66] discuss the differences in these methodologies in detail. Thus, direct comparison of the results reported in this study with those of Camras et al. is not feasible. As such, the numerical stiffness values that we report here are in good agreement with those reported by Last et al.[20] and we presume that the large elastic modulus reported for the glaucomatous TM was measured on LF regions of the TM. Studies currently are underway to confirm this.

The stiffness differences reported here are interesting, but not entirely unexpected, since we hypothesize that changes in overall outflow facility are likely associated primarily with changes within the HF regions. There are multiple possible explanations for these stiffness differences. First, the stiffness differences may be due to differences in ECM cross-linking within the regions of the TM, or alternately, due to mRNA alternative splicing or compositional difference in terms of glycosaminoglycan attachments. Increases in, or inhibition of, protein cross-linking in TM tissues has been shown recently to affect outflow facility.[67] These possibilities were not addressed in the current study, but should be investigated in future studies. Another possible explanation for the stiffness differences could be due to large differences in levels of major ECM components that previously have been shown to be located in the TM, such as fibronectin, laminin, tenascin, elastin, fibrillin-1, collagen types I, IV, V, and others.[68] As the proteomics data were from whole TM tissues, including the JCT, we were unable to correlate ECM protein differences of the whole TM with the stiffness differences measured by AFM in the deepest JCT region. Current studies are underway to separate the JCT region from the outer TM beams before performing quantitative proteomics to identify ECM protein differences within the JCT region of interest. Type VI collagen was found at higher

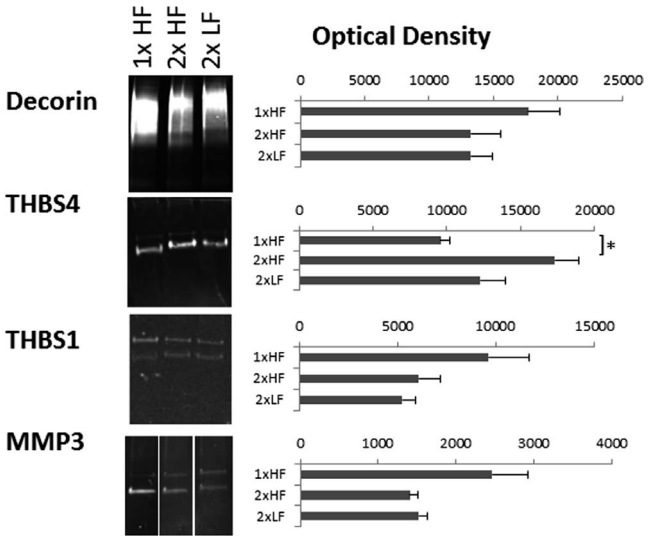

Figure 5. Western Blots of TM tissues to validate proteomics. TM tissues from perfused anterior segments were extracted and total protein concentrations were determined by BCA assay. Equal amounts of protein (15 μg/lane total protein) for each sample were run on 4% to 20% SDS-PAGE gels, transferred to PVDF membranes and probed with antibodies to MMP3, decorin, thrombospondin 4 (THBS4), or thrombospondin 1 (THBS1). (Blots were cropped at the top and bottom to improve the Fig.) Densitometry of each of the bands was plotted as units of optical density (OD). When multiple bands were present (THBS1 and MMP3), the densities of the two bands were combined for each lane. Graphs represent total OD measured in each lane. Data are average ± standard error of the mean. $N = 3$; $^*P < 0.05$.

levels in the 2× LF regions compared to 2× HF regions of the whole TM by quantitative proteomics, but it is not known whether these differences exist within the JCT region. Finally, it is possible that the stiffness differences are due to organizational changes in the TM, between LF and HF regions, as well as in HF regions in response to elevated pressure. Our proteomics results using whole TM tissue show that primarily the SLRPs and matricellular proteins were found at differential levels in LF compared to HF regions perfused at 2× pressure, or in HF regions perfused at 1× compared to 2× pressure. It is likely that there are some protein level differences in the other two comparisons, namely, 1× LF versus 1× HF, and 1× LF versus 2× LF, but these differences may be more subtle and require a much larger sample size because of biologic variability between donors and from eye to eye. Overall more proteins were associated with elevated pressure than there were associated with segmental areas of the TM by quantitative proteomics: in the comparison of 2× LF versus 2× HF, the proteomics data reflects a segmental difference that occurs only when pressure is elevated; whereas, in the 1× HF versus 2× HF comparison, the proteomics data reflect a response to elevated pressure that occurs specifically in HF regions. Collectively, these data indicate that HF regions are the primary responders to elevated pressure and that increased pressure affects HF and LF regions differently.

Because of the central role that the ECM of the TM has in maintaining aqueous outflow resistance, we were interested particularly in the ECM proteins identified at differential levels in the segmental regions and in response to elevated pressure. Interestingly, when the two differential level candidate sets were classified according to protein class, a majority of the proteins that were identified in the 2× LF versus 2× HF comparison were ECM proteins, whereas in the 1× HF versus 2× HF comparison, the majority of proteins identified were cellular components with a wide range of functions, making them difficult to link directly to outflow facility differences. In particular, the predominant class of proteins identified at differential levels in this data set were oxidoreductases, which consists of a broad functional class of proteins that catalyze redox reactions inside the cell. Many proteins identified here are mitochondrial-associated proteins, suggesting that TM cells are metabolically active in HF regions in response to elevated pressure. An interesting subset of signaling molecules also were identified in the 1× HF versus 2× HF data set and include bone morphogenetic protein 5 (BMP5), latent TGF-β binding protein 2 (LTBP2), TGF-β–induced protein (TGFBI), and the apoptosis regulator BAX, suggesting a complex response involving multiple signaling pathways in the HF regions of the TM. To determine other signaling pathways involved in response to elevated pressure via the ECM in the TM, all the ECM protein candidates were classified according to the pathways with which they are known to be associated. Type VI collagen was enriched in 2× LF regions compared to 2× HF regions and is one of many ECM proteins associated with the inflammation-mediated pathway. Multiple ECM proteins identified in the two candidate sets are associated with the integrin signaling pathway, which is triggered when integrin molecules in the cell membrane bind to ECM components resulting in actin reorganization and activation of MAPK and other signaling cascades. Recent reports have shown that Wnt signaling is responsive to ECM rigidity, likely through the integrin signaling pathway,[69,70] which has been shown previously to be associated with ECM stiffness and Wnt expression in chondrocytes,[70] as well as in human TM cells,[71,72] Therefore, it is likely to be an important pathway that may be triggered in glaucoma.

Initially, we were surprised that the ECM proteins that were found at differential levels across the whole TM did not include key structural ECM proteins. Instead, the proteins found at differential levels included a disproportionate representation of smaller proteins with roles in ECM organization and turnover, such as SLRPs and matricellular proteins. These results tell us that the organization but not the overall composition of the ECM within the whole TM, as well as the subsequent cellular responses, must be changed. This may explain the stiffness differences seen between HF and LF regions, although further quantitative proteomics must be done on the isolated JCT and Schlemm's canal region compared to the whole TM to verify this. It is interesting to note that a few of the ECM proteins identified in the proteomics from the whole TM, including decorin, lumican, TGFBI, and THBS4, showed specific localization within the JCT region of the TM by immunohistochemistry, suggesting an important role in these tissues. The proteins that were found at different levels in whole TM tissues are a select subset of proteins, including the matricellular proteins,[73–75] tenascin N, thrombospondins 1 and 4 and SLRPs, which often share matricellular protein-like behavior,[76,77] including decorin, keratocan, and lumican. SLRPs mediate interactions between integrins or other cell-associated receptors, and larger, structural ECM molecules thereby influencing structural organization in tissues.[77,78] In addition, several proteins with somewhat similar ECM organizing but less well-defined functions were included, such as, sarcospan, spondin-1, MAM domain-containing 2 (Mamcan proteoglycan), TGF-β–induced protein ig-h3 (BGH3), dermatopontin, nidogen 1 and 2, and Collagen VI. BGH3 is a TGF-β–induced protein that has a role in cell adhesion and cell-collagen interactions, whereas dermatopontin mediates cell surface integrin binding and promotes cell adhesion via interactions with fibronectin. Several proteinases often are involved in ECM turnover, including MMP2, MMP3, MMP10, as well as cathepsin G and pappalysin-1 and MMP tissue inhibitor TIMP1. Calcium

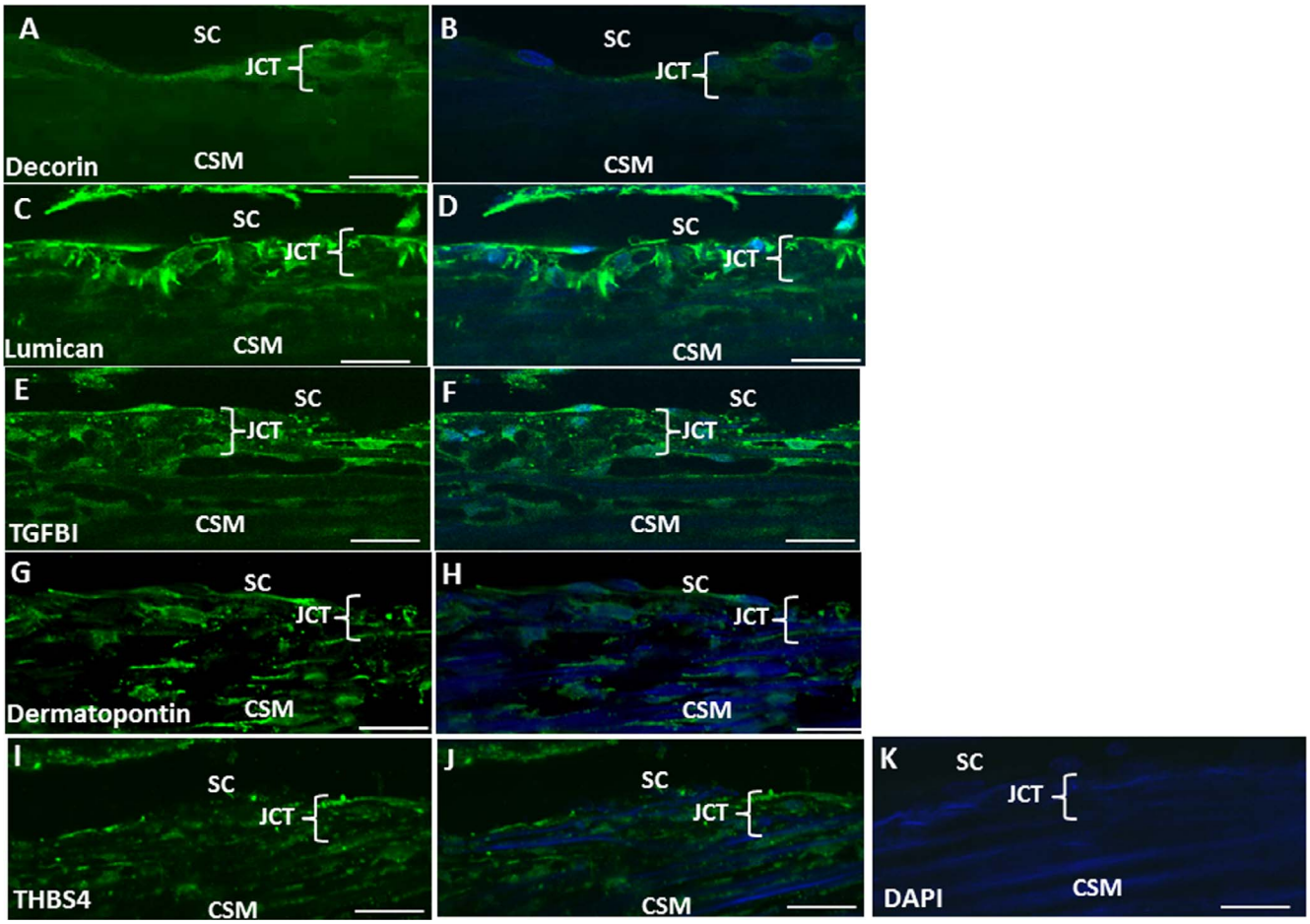

Figure 6. Immunohistochemistry of TM tissues to localize ECM proteins identified in the proteomics data. Human TM tissues from perfused anterior segments were fixed and cut tangentially before immuno-staining with antibodies to decorin (**A**, **B**), lumican (**C**, **D**), TGFBI (**E**, **F**), dermatopontin (**G**, **H**), or thromobospondin 4 (**I**, **J**). Tissues were labeled with Alexa-488 conjugated secondary antibody (green) and imaged by confocal microscopy in the presence of DAPI to visualize cell nuclei (DAPI = blue stain; [**B**, **D**, **F**, **H**, **J**, **K**]). No primary antibody control (**K**). SC, Schlemm's canal; CSM, corneoscleral TM. *Scale bar*: 20 μm for all images.

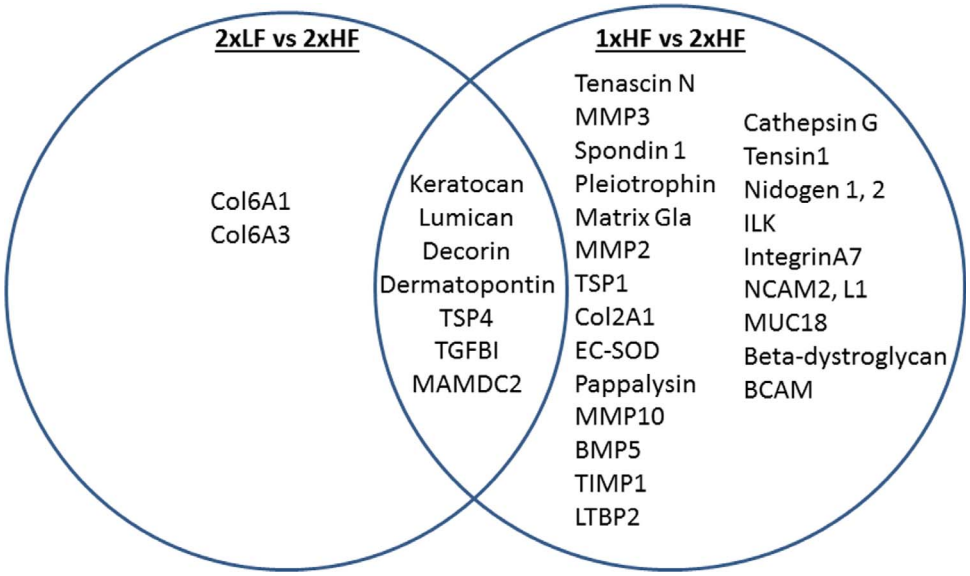

Figure 7. All ECM proteins identified at different levels in the two proteomic comparison data sets (2× LF versus 2× HF, and 1× HF versus 2× HF), and those ECM proteins common to both comparisons (*center*).

Investigative Ophthalmology & Visual Science

binding is typical for most of these ECM proteins and changes in calcium binding modulate their structures and functions dramatically. Matrix gla protein (MGP) and several other calcium-binding proteins also are present in this differences list. Decorin was one of seven ECM proteins that was enriched in the tissues of greater modulus (in the 2× LF compared to the 2× HF regions, and in the 1× HF compared to the 2× HF regions). Decorin is known to interact with a wide range of proteins from ECM molecules to cell surface receptors to growth factors and enzymes.[79] It is critical to collagen fibrillogenesis and organization in tissues, thus it's not surprising that it has an effect on the mechanical properties of tissues as has been shown in mice with a decorin deficiency.[80,81] Decorin has been shown to interact with epidermal growth factor receptor (EGFR) to attenuate downstream signaling that results in cell cycle arrest and apoptosis.[82,83] It also interacts with TGF-β, which is an important signaling molecule associated with glaucoma. Thus, it may be likely that decorin and the other ECM proteins identified in this study do not contribute directly to the mechanical properties of the TM tissue, but are involved in orchestrating the ECM turnover process, through their other properties of mediating cell–cell and cell–matrix interactions and intracellular signaling events. The changes in mechanical properties observed may be a subsequent effect of cellular responses to signaling cues. We have shown previously that ECM expression levels vary over time in their response to mechanical stretch or pressure elevation in primary cultured TM cells or in tissues.[6,10,30,84] In contrast, the proteomics data shown in this study represent only one time point: 72 hours after pressure elevation. It is clear that a complex temporal series of events must occur in response to pressure elevation, including, but not limited to ECM degradation, signal transduction, and novel biosynthesis of ECM components. Therefore, the biomechanical properties of the TM can have a strong influence on aqueous outflow, but the complexity of the response requires further studies over broader time points to fully understand the molecular mechanisms involved. This should include more detailed studies into whether longer perfusion times have an effect on apparent elastic modulus.

In conclusion, AFM data demonstrated that LF regions of the TM have higher elastic modulus (suggesting greater tissue rigidity), whereas HF regions have lower elastic modulus (more compliant) and dynamic in homeostatic response to elevated pressure. Proteomics analyses identified specific ECM protein differences in the segmental flow regions of the TM, particularly in response to elevated pressure and in the HF regions of the TM, indicating the importance of maintaining a robust response to pressure elevation as a normal function of the TM. Together these data not only provide insights into the how TM cells remodel their ECM in response to changes in pressure, but also suggest the existence of a functional network of interacting proteins that work in a coordinated manner to orchestrate ECM processes in TM tissue. The inability to respond appropriately to elevated pressure in the TM is likely to result in the development of glaucoma and lead to irreversible blindness. This work improves the understanding of the molecular mechanisms involved in the normal maintenance of the aqueous outflow pathway, which may ultimately help in the development of future therapeutics in the treatment of glaucoma.

Acknowledgments

Supported by a Bright Focus National Glaucoma Research Award (JAV, VKR), National Institute of Health (NIH; Bethesda, MD, USA) Grants EY003279, EY008247, EY025721 (TSA), P30 EY010572, and by an unrestricted grant to the Casey Eye Institute from Research to Prevent Blindness, New York, New York, United States. Mass spectrometric analysis was performed by the OHSU Proteomics Shared Resource with partial support from NIH Grants P30 EY010572, P30 OCA69533, R01 DC002368-15S1, and S10OD012246.

Disclosure: **J.A. Vranka**, None; **J.A. Staverosky**, None; **A.P. Reddy**, None; **P.A. Wilmarth**, None; **L.L. David**, None; **T.S. Acott**, None; **P. Russel**, None; **V.K. Raghunathan**, None

References

1. Quigley HA. Number of people with glaucoma worldwide. *Br J Ophthalmol*. 1996;80:389–393.
2. Quigley HA. Glaucoma. *Lancet*. 2011;377:1367–1377.
3. Rohen JW, Lutjen-Drecoll E, Flugel C, Meyer M, Grierson I. Ultrastructure of the trabecular meshwork in untreated cases of primary open-angle glaucoma (POAG). *Exp Eye Res*. 1993; 56:683–692.
4. Tektas OY, Lutjen-Drecoll E. Structural changes of the trabecular meshwork in different kinds of glaucoma. *Exp Eye Res*. 2009;88:769–775.
5. Keller KE, Acott TS. The juxtacanalicular region of ocular trabecular meshwork: a tissue with a unique extracellular matrix and specialized function. *J Ocular Biol*. 2013;1:3.
6. Acott TS, Kelley MJ, Keller KE, et al. Intraocular pressure homeostasis: maintaining balance in a high-pressure environment. *J Ocul Pharmacol Ther*. 2014;30:94–101.
7. Acott TS, Kelley MJ. Extracellular matrix in the trabecular meshwork. *Exp Eye Res*. 2008;86:543–561.
8. Keller KE, Bradley JM, Acott TS. Differential effects of ADAMTS-1, -4, and -5 in the trabecular meshwork. *Invest Ophthalmol Vis Sci*. 2009;50:5769–5777.
9. Keller KE, Bradley JM, Kelley MJ, Acott TS. Effects of modifiers of glycosaminoglycan biosynthesis on outflow facility in perfusion culture. *Invest Ophthalmol Vis Sci*. 2008;49: 2495–2505.
10. Keller KE, Kelley MJ, Acott TS. Extracellular matrix gene alternative splicing by trabecular meshwork cells in response to mechanical stretching. *Invest Ophthalmol Vis Sci*. 2007;48: 1164–1172.
11. Keller KE, Sun YY, Yang YF, Bradley JM, Acott TS. Perturbation of hyaluronan synthesis in the trabecular meshwork and the effects on outflow facility. *Invest Ophthalmol Vis Sci*. 2012; 53:4616–4625.
12. Keller KE, Vranka JA, Haddadin RI, et al. The effects of tenascin C knockdown on trabecular meshwork outflow resistance. *Invest Ophthalmol Vis Sci*. 2013;54:5613–5623.
13. Vranka JA, Kelley MJ, Acott TS, Keller KE. Extracellular matrix in the trabecular meshwork: intraocular pressure regulation and dysregulation in glaucoma. *Exp Eye Res*. 2015;133:112–125.
14. Discher DE, Janmey P, Wang YL. Tissue cells feel and respond to the stiffness of their substrate. *Science*. 2005;310:1139–1143.
15. Cox TR, Erler JT. Remodeling and homeostasis of the extracellular matrix: implications for fibrotic diseases and cancer. *Dis Model Mech*. 2011;4:165–178.
16. Bonnans C, Chou J, Werb Z. Remodelling the extracellular matrix in development and disease. *Nat Rev Mol Cell Biol*. 2014;15:786–801.
17. Handorf AM, Zhou Y, Halanski MA, Li WJ. Tissue stiffness dictates development, homeostasis, and disease progression. *Organogenesis*. 2015;11:1–15.
18. Bateman JF, Boot-Handford RP, Lamande SR. Genetic diseases of connective tissues: cellular and extracellular effects of ECM mutations. *Nat Rev Genet*. 2009;10:173–183.

Investigative Ophthalmology & Visual Science

19. Jarvelainen H, Sainio A, Koulu M, Wight TN, Penttinen R. Extracellular matrix molecules: potential targets in pharmacotherapy. *Pharmacol Rev*. 2009;61:198–223.
20. Last JA, Pan T, Ding Y, et al. Elastic modulus determination of normal and glaucomatous human trabecular meshwork. *Invest Ophthalmol Vis Sci*. 2011;52:2147–2152.
21. Camras LJ, Stamer WD, Epstein D, Gonzalez P, Yuan F. Differential effects of trabecular meshwork stiffness on outflow facility in normal human and porcine eyes. *Invest Ophthalmol Vis Sci*. 2012;53:5242–5250.
22. Camras LJ, Stamer WD, Epstein D, Gonzalez P, Yuan F. Circumferential tensile stiffness of glaucomatous trabecular meshwork. *Invest Ophthalmol Vis Sci*. 2014;55:814–823.
23. Buller C, Johnson D. Segmental variability of the trabecular meshwork in normal and glaucomatous eyes. *Invest Ophthalmol Vis Sci*. 1994;35:3841–3851.
24. Keller KE, Bradley JM, Vranka JA, Acott TS. Segmental versican expression in the trabecular meshwork and involvement in outflow facility. *Invest Ophthalmol Vis Sci*. 2011;52:5049–5057.
25. Vranka JA, Bradley JM, Yang YF, Keller KE, Acott TS. Mapping molecular differences and extracellular matrix gene expression in segmental outflow pathways of the human ocular trabecular meshwork. *PLoS One*. 2015;10:e0122483.
26. Cha ED, Xu J, Gong L, Gong H. Variations in active outflow along the trabecular outflow pathway. *Exp Eye Res*. 2016;146:354–360.
27. Swaminathan SS, Oh DJ, Kang MH, Rhee DJ. Aqueous outflow: segmental and distal flow. *J Cataract Refract Surg*. 2014;40:1263–1272.
28. Chang JY, Folz SJ, Laryea SN, Overby DR. Multi-scale analysis of segmental outflow patterns in human trabecular meshwork with changing intraocular pressure. *J Ocul Pharmacol Ther*. 2014;30:213–223.
29. Vittal V, Rose A, Gregory KE, Kelley MJ, Acott TS. Changes in gene expression by trabecular meshwork cells in response to mechanical stretching. *Invest Ophthalmol Vis Sci*. 2005;46:2857–2868.
30. Johnson DH, Tschumper RC. Human trabecular meshwork organ culture. A new method. *Invest Ophthalmol Vis Sci*. 1987;28:945–953.
31. Acott TS, Kingsley PD, Samples JR, Van Buskirk EM. Human trabecular meshwork organ culture: morphology and glycosaminoglycan synthesis. *Invest Ophthalmol Vis Sci*. 1988;29:90–100.
32. Tamm ER, Siegner A, Baur A, Lutjen-Drecoll E. Transforming growth factor-beta 1 induces alpha-smooth muscle-actin expression in cultured human and monkey trabecular meshwork. *Exp Eye Res*. 1996;62:389–397.
33. Morgan JT, Raghunathan VK, Thomasy SM, Murphy CJ, Russell P. Robust and artifact-free mounting of tissue samples for atomic force microscopy. *Biotechniques*. 2014;56:40–42.
34. Raghunathan VK, Morgan JT, Park SA, et al. Dexamethasone Stiffens trabecular meshwork, trabecular meshwork cells, and matrix. *Invest Ophthalmol Vis Sci*. 2015;56:4447–4459.
35. Zeng D, Juzkiw T, Read AT, et al. Young's modulus of elasticity of Schlemm's canal endothelial cells. *Biomech Model Mechanobiol*. 2010;9:19–33.
36. Vargas-Pinto R, Gong H, Vahabikashi A, Johnson M. The effect of the endothelial cell cortex on atomic force microscopy measurements. *Biophys J*. 2013;105:300–309.
37. Vajabikashi A, Dong B, Zhang HF, Johnson M. In Situ stiffness characterization of the human inner wall endothelium of Schlemm's canal and its substrate. *ISER/BrightFocus 2017 Glaucoma Symposium*. Atlanta, GA; 2017:141.
38. McKee CT, Last JA, Russell P, Murphy CJ. Indentation versus tensile measurements of Young's modulus for soft biological tissues. *Tissue Eng Part B Rev*. 2011;17:155–164.
39. Anseth KS, Bowman CN, Brannon-Peppas L. Mechanical properties of hydrogels and their experimental determination. *Biomaterials*. 1996;17:1647–1657.
40. Dimitriadis EK, Horkay F, Maresca J, Kachar B, Chadwick RS. Determination of elastic moduli of thin layers of soft material using the atomic force microscope. *Biophys J*. 2002;82:2798–2810.
41. Vinckier A, Semenza G. Measuring elasticity of biological materials by atomic force microscopy. *FEBS Lett*. 1998;430:12–16.
42. Ahearne M, Yang Y, El Haj AJ, Then KY, Liu KK. Characterizing the viscoelastic properties of thin hydrogel-based constructs for tissue engineering applications. *J R Soc Interface*. 2005;2:455–463.
43. Herrmann LR. Elasticity equations for incompressible and nearly incompressible materials by a variational theorem. *AIAA J*. 1965;3:1896–1900.
44. Mahaffy RE, Shih CK, MacKintosh FC, Kas J. Scanning probe-based frequency-dependent microrheology of polymer gels and biological cells. *Phys Rev Lett*. 2000;85:880–883.
45. Erde J, Loo RR, Loo JA. Enhanced FASP (eFASP) to increase proteome coverage and sample recovery for quantitative proteomic experiments. *J Proteome Res*. 2014;13:1885–1895.
46. Kall L, Canterbury JD, Weston J, Noble WS, MacCoss MJ. Semi-supervised learning for peptide identification from shotgun proteomics datasets. *Nat Methods*. 2007;4:923–925.
47. Plubell DL, Wilmarth PA, Zhao Y, et al. Extended multiplexing of tandem mass tags (TMT) labeling reveals age and high fat diet specific proteome changes in mouse epididymal adipose tissue. *Mol Cell Proteomics*. 2017;16:873–890.
48. Robinson MD, McCarthy DJ, Smyth GK. edgeR: a bioconductor package for differential expression analysis of digital gene expression data. *Bioinformatics*. 2010;26:139–140.
49. Robinson MD, Oshlack A. A scaling normalization method for differential expression analysis of RNA-seq data. *Genome Biol*. 2010;11:R25.
50. Vizcaíno JA, Côté RG, Csordas A, et al. The PRoteomics IDEntifications (PRIDE) database and associated tools: status in 2013. *Nucleic Acids Res*. 2013;41:D1063–D1069.
51. Mi H, Dong Q, Muruganujan A, Gaudet P, Lewis S, Thomas PD. PANTHER version 7: improved phylogenetic trees, orthologs and collaboration with the Gene Ontology Consortium. *Nucleic Acids Res*. 2010;38:D204–210.
52. Mi H, Guo N, Kejariwal A, Thomas PD. PANTHER version 6: protein sequence and function evolution data with expanded representation of biological pathways. *Nucleic Acids Res*. 2007;35:D247–252.
53. Mi H, Huang X, Muruganujan A, et al. PANTHER version 11: expanded annotation data from Gene Ontology and Reactome pathways, and data analysis tool enhancements. *Nucleic Acids Res*. 2017;45:D183–D189.
54. Mi H, Muruganujan A, Casagrande JT, Thomas PD. Large-scale gene function analysis with the PANTHER classification system. *Nat Protoc*. 2013;8:1551–1566.
55. Mi H, Poudel S, Muruganujan A, Casagrande JT, Thomas PD. PANTHER version 10: expanded protein families and functions, and analysis tools. *Nucleic Acids Res*. 2016;44:D336–342.
56. Mi H, Thomas P. PANTHER pathway: an ontology-based pathway database coupled with data analysis tools. *Methods Mol Biol*. 2009;563:123–140.
57. Lu Z, Overby DR, Scott PA, Freddo TF, Gong H. The mechanism of increasing outflow facility by rho-kinase inhibition with Y-27632 in bovine eyes. *Exp Eye Res*. 2008;86:271–281.
58. Swaminathan SS, Oh DJ, Kang MH, et al. Secreted protein acidic and rich in cysteine (SPARC)-null mice exhibit more

Investigative Ophthalmology & Visual Science

uniform outflow. *Invest Ophthalmol Vis Sci*. 2013;54:2035–2047.

59. Raghunathan VK, Morgan JT, Dreier B, et al. Role of substratum stiffness in modulating genes associated with extracellular matrix and mechanotransducers YAP and TAZ. *Invest Ophthalmol Vis Sci*. 2013;54:378–386.
60. Stamer WD, Acott TS. Current understanding of conventional outflow dysfunction in glaucoma. *Curr Opin Ophthalmol*. 2012;23:135–143.
61. Wang K, Read AT, Sulchek T, Ethier CR. Trabecular meshwork stiffness in glaucoma. *Exp Eye Res*. 2017;158:3–12.
62. Furuyoshi N, Furuyoshi M, Futa R, Gottanka J, Lutjen-Drecoll E. Ultrastructural changes in the trabecular meshwork of juvenile glaucoma. *Ophthalmologica*. 1997;211:140–146.
63. Johnson D, Gottanka J, Flugel C, Hoffmann F, Futa R, Lutjen-Drecoll E. Ultrastructural changes in the trabecular meshwork of human eyes treated with corticosteroids. *Arch Ophthalmol*. 1997;115:375–383.
64. Rohen JW, Lutjen-Drecoll E. Age changes of the trabecular meshwork in human and monkey eyes. A light and electron microscopic study. *Altern Entwickl Aging Dev*. 1971;1:1–36.
65. Schlunck G, Han H, Wecker T, Kampik D, Meyer-ter-Vehn T, Grehn F. Substrate rigidity modulates cell matrix interactions and protein expression in human trabecular meshwork cells. *Invest Ophthalmol Vis Sci*. 2008;49:262–269.
66. Raghunathan VK. Biomechanics and the aqueous humor outflow pathway. In: Knepper PA, Samples JR, eds. *Glaucoma Research and Clinical Advances 2016 to 2018*. Amsterdam, The Netherlands: Kugler Publications; 2016:121–138.
67. Yang YF, Sun YY, Acott TS, Keller KE. Effects of induction and inhibition of matrix cross-linking on remodeling of the aqueous outflow resistance by ocular trabecular meshwork cells. *Sci Rep*. 2016;6:30505.
68. Ueda J, Wentz-Hunter K, Yue BY. Distribution of myocilin and extracellular matrix components in the juxtacanalicular tissue of human eyes. *Invest Ophthalmol Vis Sci*. 2002;43:1068–1076.
69. Barbolina MV, Liu Y, Gurler H, et al. Matrix rigidity activates Wnt signaling through down-regulation of Dickkopf-1 protein. *J Biol Chem*. 2013;288:141–151.
70. Du J, Zu Y, Li J, et al. Extracellular matrix stiffness dictates Wnt expression through integrin pathway. *Sci Rep*. 2016;6:20395.
71. Faralli JA, Gagen D, Filla MS, Crotti TN, Peters DM. Dexamethasone increases alphavbeta3 integrin expression and affinity through a calcineurin/NFAT pathway. *Biochim Biophys Acta*. 2013;1833:3306–3313.
72. Faralli JA, Newman JR, Sheibani N, Dedhar S, Peters DM. Integrin-linked kinase regulates integrin signaling in human trabecular meshwork cells. *Invest Ophthalmol Vis Sci*. 2011;52:1684–1692.
73. Bornstein P, Sage EH. Matricellular proteins: extracellular modulators of cell function. *Curr Opin Cell Biol*. 2002;14:608–616.
74. Chatterjee A, Villarreal G Jr, Rhee DJ. Matricellular proteins in the trabecular meshwork: review and update. *J Ocul Pharmacol Ther*. 2014;30:447–463.
75. Murphy-Ullrich JE, Sage EH. Revisiting the matricellular concept. *Matrix Biol*. 2014;37:1–14.
76. Merline R, Schaefer RM, Schaefer L. The matricellular functions of small leucine-rich proteoglycans (SLRPs). *J Cell Commun Signal*. 2009;3:323–335.
77. Schaefer L, Iozzo RV. Biological functions of the small leucine-rich proteoglycans: from genetics to signal transduction. *J Biol Chem*. 2008;283:21305–21309.
78. Chen S, Birk DE. The regulatory roles of small leucine-rich proteoglycans in extracellular matrix assembly. *FEBS J*. 2013;280:2120–2137.
79. Gubbiotti MA, Vallet SD, Ricard-Blum S, Iozzo RV. Decorin interacting network: a comprehensive analysis of decorin-binding partners and their versatile functions. *Matrix Biol*. 2016;55:7–21.
80. Robinson PS, Huang TF, Kazam E, Iozzo RV, Birk DE, Soslowsky LJ. Influence of decorin and biglycan on mechanical properties of multiple tendons in knockout mice. *J Biomech Eng*. 2005;127:181–185.
81. Zhang G, Ezura Y, Chervoneva I, et al. Decorin regulates assembly of collagen fibrils and acquisition of biomechanical properties during tendon development. *J Cell Biochem*. 2006;98:1436–1449.
82. Goldoni S, Iozzo RV. Tumor microenvironment: modulation by decorin and related molecules harboring leucine-rich tandem motifs. *Int J Cancer*. 2008;123:2473–2479.
83. Seidler DG, Goldoni S, Agnew C, et al. Decorin protein core inhibits in vivo cancer growth and metabolism by hindering epidermal growth factor receptor function and triggering apoptosis via caspase-3 activation. *J Biol Chem*. 2006;281:26408–26418.
84. Vranka JA, Acott TS. Pressure-induced expression changes in segmental flow regions of the human trabecular meshwork. *Exp Eye Res*. 2017;158:67–72.

Investigative Ophthalmology & Visual Science